Available online at www.sciencedirect.com

SciVerse ScienceDirect

Ceramics International 39 (2013) 2437–2442

CERAMICS INTERNATIONAL

www.elsevier.com/locate/ceramint

Nanostructured ceramic composite coating prepared by reactive plasma spraying micro-sized Al–Fe_2O_3 composite powders

Lei Wang*, Dianran Yan, Yanchun Dong, Jianxin Zhang, Xueguang Chen

Key Laboratory for New Type of Functional Materials in Hebei Province, School of Materials Science and Engineering, Hebei University of Technology, Tianjin, China

Received 6 August 2012; received in revised form 30 August 2012; accepted 31 August 2012
Available online 7 September 2012

Abstract

Nanostructured ceramic matrix composite coating was prepared in-situ by reactive plasma spraying micro-sized Al-Fe_2O_3 composite powders. The microstructure, toughness and Vickers hardness of these coatings were investigated by X-ray diffraction, scanning electron microscopy, transmission electron microscopy and mechanical tests. The results indicated that the coating exhibited nanostructures which consisted of $FeAl_2O_4$, Al_2O_3, Fe (or Fe solid solution) and a little FeAl. The composite coating showed significantly higher toughness and wear resistance than the conventional Al_2O_3 coating.

Keywords: Composite coating; Nanostructured coating; Reactive plasma spraying; Thermite reaction

1. Introduction

Coating is a unique way to tailor the surface properties of a component to suit a specific environment without sacrificing the bulk characteristics. Thermal plasma technology is increasingly applied to a variety of materials processing applications [1–3]. Thermite reactions have become important in the synthesis of refractory ceramic and composite materials and in the preparation of ceramic coatings in metallic pipes [4]. The thermite reaction between Fe_2O_3 and Al has been extensively studied and developed to be applied in welding, producing composites and fabricating alumina coatings inside metal pipes under centrifugal force [5–7]. Because of the large exothermic heat, the thermite reaction can generally be initiated locally and can become self-sustaining, which makes their use extremely energy efficient. Reactive plasma spraying combines plasma spraying with self-propagating high-temperature synthesis to produce in-situ composite coatings [8–11]. In recent years, development of nanocrystalline/nanostructured coating has attracted significant scientific and industrial interest. It is generally believed that, because of their ultrafine structures, the coatings would exhibit novel properties compared to traditional materials and open up opportunities for new technological applications [12–14]. In the present paper, the formation of an in-situ high-performance nanostructured ceramic matrix composites (CMC) coating toughed by metallic phase through reactive plasma spraying microstructured Al/Fe_2O_3 composite powders was investigated. The microstructure and mechanical properties of the as-sprayed nanostructured CMC coating and traditional Al_2O_3 coating were carefully characterized and compared.

2. Experimental procedures

The present investigation is based on the following reaction:

$$Fe_2O_3 + 2Al \rightarrow Al_2O_3 + 2Fe + 836\ kJ$$

The reagents used in this study consisted of commercial powders of Al and Fe_2O_3. The pure Fe_2O_3 power is produced by Tianjin Third Chemical Reagent Co., Ltd., China. The average particle size of Fe_2O_3 powder is about 0.6–0.8 μm. The pure Al powder is made by Anshan Iron and Steel Fine Aluminum Powder Co., Ltd., China and the average particle size is 4–5 μm. Fe_2O_3 and Al powders were

*Corresponding author.
E-mail addresses: wleilei@hebut.edu.cn, wleilei1@163.com (L. Wang).

0272-8842/$ - see front matter © 2012 Elsevier Ltd and Techna Group S.r.l. All rights reserved.
http://dx.doi.org/10.1016/j.ceramint.2012.08.095

wet-mixed thoroughly by grinding with addition of polyvinyl alcohol as binder using a mortar in a molar ratio of 1:2. The feedstock powders employed in this work were engineered to exhibit similar particle size distribution (50–75 μm) in order to generate similar values of particle temperature and velocity in the spray jet. The substrate is carbon steel (0.14–0.22 wt% C) which was machined into sample of 30 mm × 25 mm × 10 mm. The steel was degreased and grit-blasted by using alumina grit with a pressure-operated machine to give a surface roughness (Ra > 25 μm) immediately before spraying. A bond coating of Ni–10 wt%Al self-melting alloy with thickness about 100 μm was deposited onto the carbon steel substrates in order to increase the adhesive strength between the composite coating and the substrate. The as-prepared Al–Fe_2O_3 composite powders and conventional microstructured monolithic Al_2O_3 powder were then plasma sprayed onto the bond coatings for about 300 μm in thickness respectively. The coating was sprayed using GDP-2 type 50 kW plasma spraying device made by Jiu Jiang Spraying Device Company, China. Fig. 1 shows the schematic drawing of the reactive spraying process. The spraying processing parameters are given in Table 1.

Powder morphology, surface and cross-section topography of the coatings were examined using the PHILIPS XL30 scanning electron microscope (SEM) equipped with energy dispersive X-ray spectroscopy (EDS). The Philips X,-pert MPD X-ray diffraction instrument with Cu Kα target was used to identify the phases and compositions of the composite powders and the coating. The microstructure of the coating was characterized by transmission electron microscope (TEM, Philips Tec- nai F20). The microhardness was determined on the polished cross-section of the coatings by a HX-1000 Microhardness tester under an indent load of 100 gf with a dwell time of 15 s. An average of 10 tests was used as an indicator of the coating hardness. Relative toughness of the coatings is expressed by crack extension force (G_c) calculated from Eq. (1) [15]

$$G_c = 6.115 \times 10^{-4}(a^2 P/c^3) \quad (1)$$

where, G_c: the crack extension force (J m^{-2}); a: the impression half-diagonal (m); P: the indentation load (N); c: the half of the total length (tip-to-tip) of the major crack.

The wear volume was determined using the wear track data measured by the profile meter. Commercial GCr15 steel rings (HRC 62) were used to rotate in contact with each block sample. At least three specimens were tested for each load to obtain the average value.

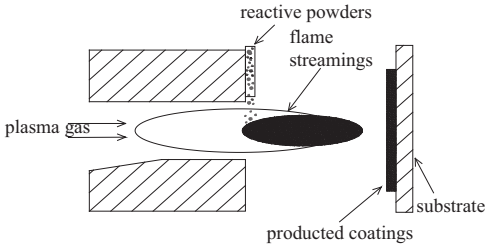

Fig. 1. Schematic of the reactive plasma spraying gun.

3. Results and discussion

3.1. Characterization of the composite powders

Fig. 2(a) shows the BSE images of the Al/Fe_2O_3 composite powders. It is found that the powders present quasi-spherical shape after reconstitution process. The average particle diameter of the composite powders is about 50 μm. In the powder, the Al particulates are uniformly clad by fine Fe_2O_3 particles, which will be beneficial to the thermite reaction between Fe_2O_3 and Al particles and thus the homogeneous composition distribution of the coating is obtained. The XRD pattern of the composite powders is presented in Fig. 2(b). From which, it is clearly observed that the composite powders consisted of Fe_2O_3 and Al phases, and no other phases are detected, which indicates that the composite powders kept high stability during the reconstitution process.

3.2. Phase and microstructure analysis of the CMC coating

Fig. 3(a) shows the XRD pattern of the CMC coating. It is found that the coating is composed of $FeAl_2O_4$, Fe, Al_2O_3 and a little FeAl, the main phases are Fe and $FeAl_2O_4$ spinel. No pure Al or Fe_2O_3 phase can be detected in the coating, which means Al and Fe_2O_3 have reacted completely. Fig. 3(b) shows the BSE images of cross-section morphology of the CMC coating. The coating presents a typical lamellar microstructure with little porosity and these splats are tightly stacked. It can be seen that the CMC coating contains four distinctive regions, namely white region (A), light grain region (B), dark grain region (C) and black region (D), which are uniformly overlapped. The EDS results of corresponding regions are shown in Table 2. From the EDS and XRD results, it can be found that the white region (zone A) is Fe-rich phase;

Table 1
Process parameters of plasma spraying.

Ar (L/min)	H_2 (L/min)	Input current (A)	Voltage (V)	Spray distance (mm)	The anode nozzle internal diameter (i.d.) (mm)	Injector nozzle i.d. (mm)	Injector position	Carrier gas flow rate (L/min)
80	20	500	60	100	8	3	Radial, outside of the nozzle	8

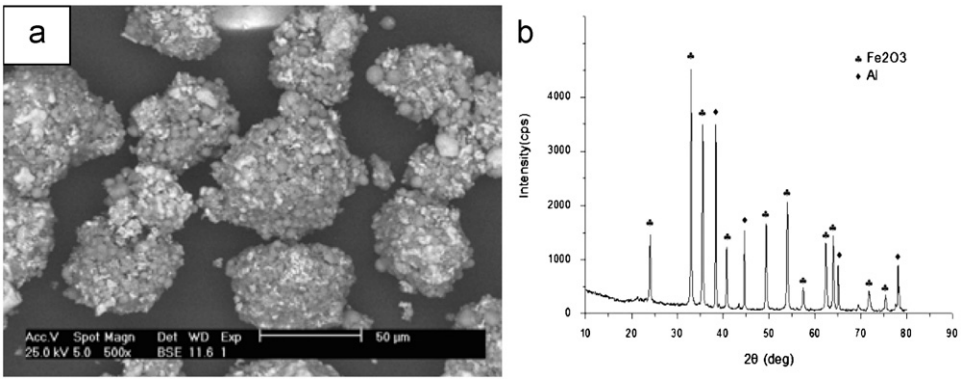

Fig. 2. SEM micrograph and XRD pattern of the Fe_2O_3/Al composite powders: (a) BSE micrograph; (b) XRD pattern.

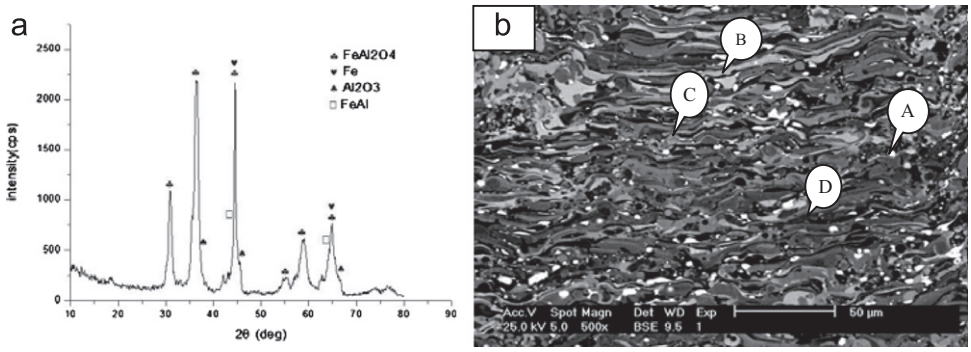

Fig. 3. (a) XRD patterns of the CMC coating, (b) BSE micrograph of cross-sectional CMC coating.

Table 2
Corresponding EDS results of four regions in Fig. 3b.

	Fe (at%)	Al (at%)	O (at%)
A	91.33	3.29	5.38
B	27.34	33.79	38.87
C	11.97	49.37	38.66
D	5.95	52.81	41.24

the gray zones B and C are $FeAl_2O_4$-rich phases and the black zone D is Al_2O_3-rich phase. Thus, it can be concluded that the microstructure of the CMC coating consists of phases with different morphologies. As the matrix, the gray $FeAl_2O_4$-rich phase possesses lamellar splat microstructure. As second phases, the granular Fe-rich metal particles and the black thin lamellar splats of Al_2O_3-rich phase are embedded into the $FeAl_2O_4$-rich phase matrix.

The TEM bright field images and the corresponding selected area diffraction (SAD) patterns of the CMC coating are displayed in Fig. 4. The CMC coating consists of a large number of nano-sized grains with different morphology, which are on the order of tens of nanometers to hundreds of nanometers. Fig. 4a shows equiaxed micrograins (diameter about 50–200 nm) and columnar grains (diameter about 50–100 nm) in the composite coatings. Fig. 4b is the higher magnified TEM micrograph of the columnar nanograins. The SAD patterns of two microstructures are indexed to be $FeAl_2O_4$. There are a lot of spherical grains (size about 50–100 nm) which are embedded in the $FeAl_2O_4$ matrix (Fig. 4a). The SAD pattern of the spherical grain suggests that spherical grains are α-Fe phase (Fig. 4c). There are also a lot of spherical grains with the size about 10–60 nm embedded in the matrix (Fig. 4d), and the SAD pattern indicates that these spherical grains are γ-Al_2O_3. The TEM characterization revealed a lot of spherical α-Fe and γ-Al_2O_3 nano-grains embedded in the equiaxed and columnar $FeAl_2O_4$ nano-grains matrix.

3.3. Microhardness and toughness

With increasing applied loads which ranged from 100 gf to 1000 gf, the Vickers microhardness of the coating exhibits a slow drop-down tendency from 895 Hv_{100} to 775 Hv_{1000} as shown in Fig. 5.

It is obvious that such phenomenon reveals a typical indentation size effect (ISE) [16]. Due to presence of softer $FeAl_2O_4$ and Fe phases in the coating, the microhardness of the CMC coating is 895 ± 15 HV, which is lower than that of conventional microstructured monolithic Al_2O_3 coating developed using plasma spraying process (1070 ± 40 HV). The calculated crack extension force of CMC coating is approximately 10.1 J/m^2, which is 20% higher than that of the nanostructured $Al_2O_3+13\%TiO_2$ coating (8.4 J/m^2) and twice higher than microstructured Al_2O_3 coating (5.4 J/m^2) deposited by plasma spraying process. Fig. 6(a) and (b) show Vickers-hardness indentations of the Al_2O_3 coatings and

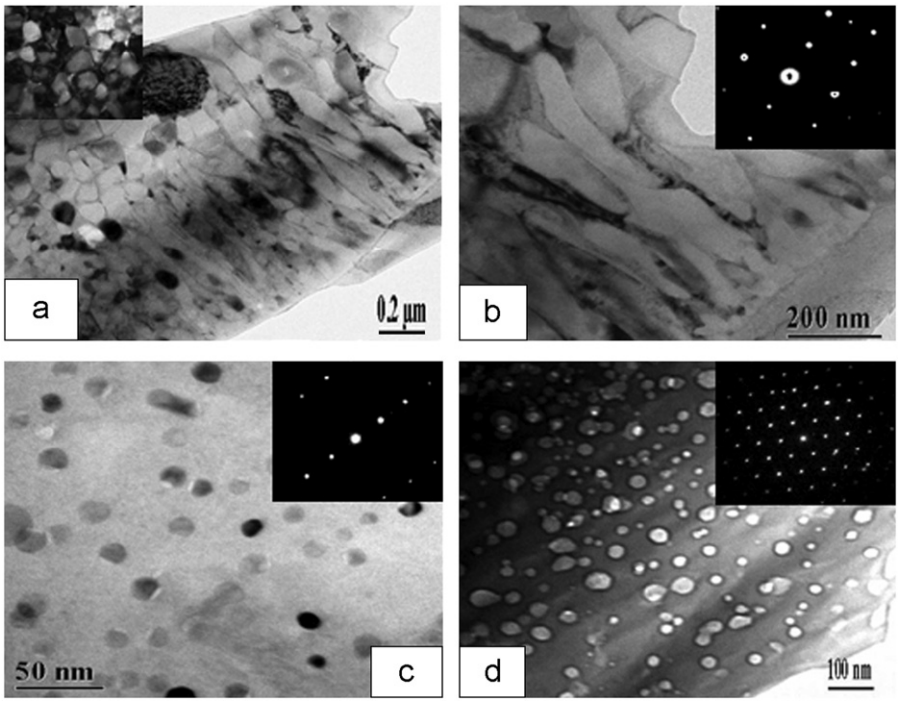

Fig. 4. TEM morphology of the reactive plasma sprayed composite coating (a) spherical nanocrystalline and equiaxed $FeAl_2O_4$ nano-grains, (b) columnar $FeAl_2O_4$ nano-grains, (c) spherical α-Fe nano-grains, (d) spherical γ-Al_2O_3 nano-grains.

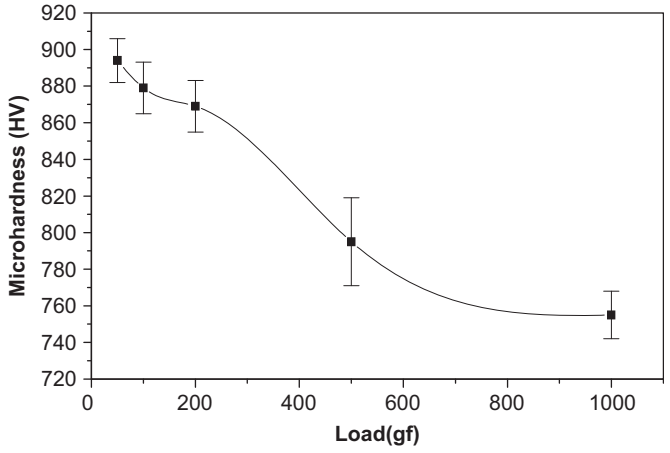

Fig. 5. Dependence of Vickers microhardness values at different loads for the CMC coating.

composite coatings at load of 100 gf. It can be seen that the Al_2O_3 coating is broken along the edge of the indentation impression (Fig. 6a), and multiple cracking is present around the indentation impression. However, few microcracks are formed around the indentation impression on the CMC coating (Fig. 6b). The indentation impression with clear shape and fewer microcracks on the CMC coating exhibits more ductile behavior than Al_2O_3 coating. It is known that Al_2O_3 is a hard but brittle phase, and stress concentration and fine cracks can easily form when the Al_2O_3 coating withstand the pressure. In contrast, the presence of tough and ductile Fe phase in the CMC coating can efficiently prevent the stress concentration and absorb the fracture energy. It is confirmed that combination of the nanostructured ceramic and the ductile Fe phase can improve the ductility of the ceramic coating.

3.4. Fractographic characterization of the CMC coating

The SEM micrographs of the fracture surfaces of the Al_2O_3 coating and CMC coating are shown in Fig. 7. There are two morphologies in Al_2O_3 coating, one is the facet as shown in A of Fig. 7(a) and the other is typical step which is formed in the process of cleavage fracture and shown in B of Fig. 7(a). Al_2O_3 particles do not completely melt during the plasma spraying, causing the lower bonding strength of the coating. The rapture exhibits the facet micrographs which are similar to the intercrystalline cracking formed in the particles or in the lamellar splat. Hence, the fracture mode of the Al_2O_3 coating that is mainly composed of cleavage fracture is brittle fracture.

It can be seen from Fig. 7(b) that the lamellar splats of the CMC coating are thinner and better-knit than that of the Al_2O_3 coating. The CMC coating exhibits more ductile mode of fracture compared with the Al_2O_3 coating, which is illustrated by relatively larger number of dimples (Fig. 7(b) A and B) in the fractograph possibly left by the extracting of the metallic Fe particles. The B and C areas of Fig. 7(C) are the residue of the rapture metal particles. Fig. 7(c) is BSE micrograph of the fracture corresponding to the area of B and C in Fig. 7(b). Some metal particles are involved in the fracture of the coating, and the other particles are extracted from the matrix during the fracture process. The in situ synthesized metal second phase particles dispersed in the coating can service as micro-absorbers to prevent the stress

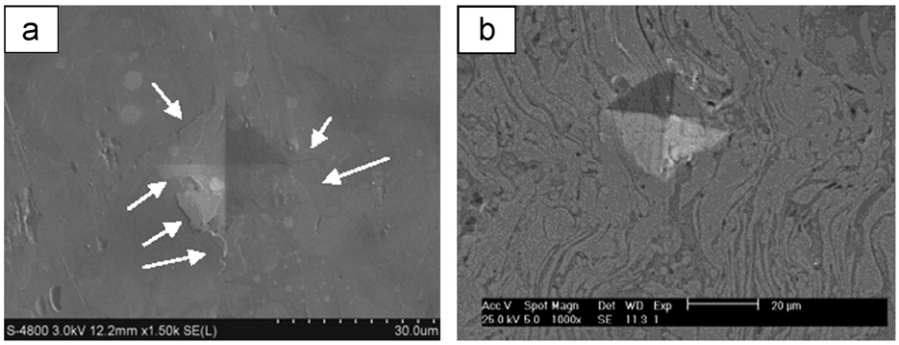

Fig. 6. Vickers-hardness indentations at load of 100 gf of: (a) Al_2O_3 coating; (b) CMC coating.

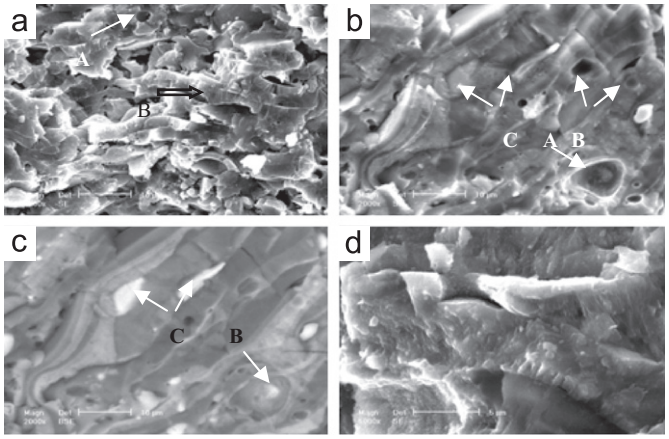

Fig. 7. Micrographs of the fracture surfaces of coatings (a) Al_2O_3 coating, (b) CMC coating, (c) BSE micrographs of CMC coating, (d) high magnified fracture micrograph of CMC coating.

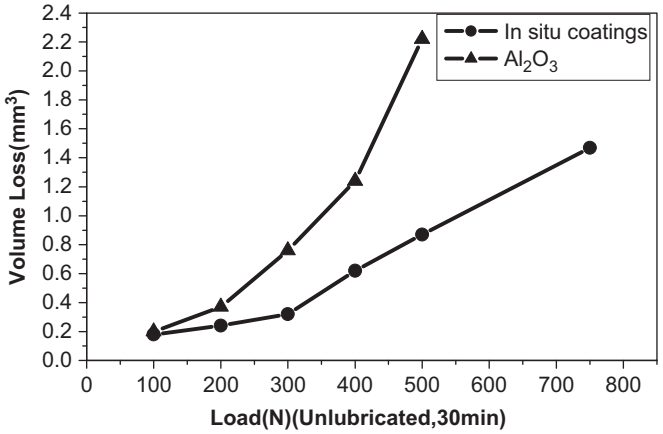

Fig. 8. Wear volume loss of the composite coating and Al_2O_3 coating plotted as a function of loads.

concentration and absorb the fracture energy. When loads are put on the coatings, the micro-absorbers will generate the plastic deformation in a certain degree.

Furthermore, dispersed metal particles can work as bridge between the ceramic matrix to buffer and deflect microcrack propagation [15], as shown in Fig. 7(b). Accordingly, the microcracks had to walk a farther route when they bypass the metal phase. Compared with the monophase ceramic material, the in situ synthesized metal second phase will lead to complex fracture behavior that mixed intergranular and transgranular fracture modes (see in Fig. 7(b)) due to the composite microstructure of mixed metal and ceramic phase mixture. The dissipation of energy originated from the plastic deformation of the metal second phase is considered as the most essential toughening factor. Additionally, the relatively higher fraction and homogeneous dispersion of metal phase in the CMC coating will devote to toughness enhancement.

3.5. Frictional wear test

Fig. 8 shows the wear volume of Al_2O_3 coating and CMC coating against GCr15 steel at different loads. With increasing loads, the wear volumes of the two coatings increase. The wear volume of the CMC coating is lower than that of the Al_2O_3 coating under the same load, especially under high load. The wear volume of the CMC coating is only 1/2 of that of Al_2O_3 coating under normal load of 500 N. The preferable toughness of the CMC coating remarkably improves its wear resistance. The in situ synthesized metal second phase particles dispersed within the coating can efficiently prevent the stress concentration and absorb the fracture energy.

Tribological heat produced by friction during testing is difficult to diffuse, so it will concentrate on the real contact area of friction pairs, which will raise the temperature of the Al_2O_3 coating quickly and accelerate the wear of the Al_2O_3 coating [16]. Metallic phase Fe in the CMC coating is an excellent conductor of heat, so the temperature increase of the CMC coating is relatively low, which led to the lower wear volume of the CMC coating. It is known that the smaller the grain size, the higher the external stress required to induce grain boundary cracking and grain pulling out [17]. Refining the coating microstructure to nanostructure will improve the ductility of the CMC coating [18]. The enhanced grain boundary adhesive strength between second phases and matrix due to in situ natural formation of all phases is also contributing to the better wear resistance of the CMC coating compared with the Al_2O_3 coating [19]. Therefore, the CMC coating presents excellent wear resistance.

4. Conclusion

Nanostructured ceramic matrix composite coating was successfully deposited in-situ by reactive plasma spraying micro-sized Al/Fe_2O_3 composite powders. The composite coating exhibited dense microstructure with a number of spherical α-Fe and γ-Al_2O_3 nano-grains embedded in the equiaxed and columnar $FeAl_2O_4$ nano-grains matrix, and it was found that the in situ synthesized metal phase was helpful to toughen the coating matrix. The composite coating exhibited excellent toughness and anti-friction in comparison with conventional Al_2O_3 monophase coating, though its microhardness value was a little lower than that of Al_2O_3 coating, which were attributed to the nanostructure of the composite coating and the inclusion of ductile metallic phase of Fe in the composite coating.

Acknowledgment

The authors gratefully acknowledge the financial supports of the National Natural Science Foundation of China (Grant Nos. 51072045 and 51102074), Doctoral Program Specialized Research Foundation for Universities in China (Grant No. 20101317120005) and China Postdoctoral Science Foundation (Grant No. 20110490979).

References

[1] P.V. Anathapadmanabhan, T.K. Thiyagarajan, K.P. Sreekumar, N. Venkatramani, Formation of nano-sized alumina by in-flight oxidation of aluminium powder in a thermal plasma reactor, Scripta Materialia 50 (1) (2004) 143–147.

[2] Serdar Salman, Ramazan Köse, Levent Urtekin, Fehim Findik, An investigation of different ceramic coating thermal properties, Materials & Design 26 (2007) 585–590.

[3] N.H.N. Yusoff, M.J. Ghazali, M.C. Isa, A.R. Daud, A. Muchtar, Optimization of plasma spray parameters on the mechanical properties of agglomerated Al_2O_3 –13%TiO_2 coated mild steel, Materials & Design 39 (2012) 504–508.

[4] J. Mei, R.D. Halldear, P. Xiao, Mechanisms of the aluminium–iron oxide thermite reaction, Scripta Materialia 41 (5) (1999) 541–548.

[5] R.S. Lima, B.R. Marple, Journal of Thermal Spray Technology 16 (1) (2007) 40–63.

[6] Luísa Durães, Benilde F.O. Costa, Regina Santos, Fe_2O_3/aluminum thermite reaction intermediate and final products characterization, Materials Science and Engineering: A 4659 (1–2) (2007) 199–210.

[7] Wuhrer, W.Y. Yeung, Grain refinement with increasing magnetron discharge power in sputter deposition of nanostructured titanium aluminium nitride coatings, Scripta Materialia 50 (6) (2004) 813–818.

[8] Lisong Xiao, Dianran Yan, Lin Zhu, Yanchun Dong, Nanostructured TiN coating prepared by reactive plasma spraying in atmosphere, Applied Surface Science 253 (18) (2007) 7535–7539.

[9] Akira Kobayashi, Formation of TiN coatings by gas tunnel type plasma reactive spraying, Surface and Coatings Technology 132 (2–3) (2000) 152–157.

[10] Lidong Zhao, Lugscheider Erich, Reactive plasma spraying of $TiAl_6V_4$ alloy, Wear 253 (11–12) (2002) 1214–1218.

[11] Dongli Zou, Dianran Yan, Lisong Xiao, Yanchun Dong, Characterization of nanostructured TiN coatings fabricated by reactive plasma spraying, Surface and Coatings Technology 202 (10) (2008) 1928–1934.

[12] A.K. Basak, S. Achanta, J.P. Celis, Structure and mechanical properties of plasma sprayed nanostructured alumina and FeCuAl–alumina cermet coatings, Surface and Coatings Technology 202 (11) (2008) 2368–2373.

[13] Vinay Pratap Singh, Anjan Sil, R. Jayaganthan, A study on sliding an erosive wear behavior of atmospheric plasma sprayed conventional and nanostructured alumina coatings, Materials & Design 32 (2) (2011) 584–591.

[14] Huangchen, Yefan Zhang, Chuanxian Ding, Tribological properties of nanostructured zirconia coatings deposited by plasma spraying, Wear 253 (7–8) (2002) 885–893.

[15] Zoiss D, Lekatou A, Varadavoulias M, A microstructure and mechanical property investigation on thermally sprayed nanostructured ceramic coatings before and after a sintering treatment, Surface and Coatings Technology 204 (1–2) (2009) 15–27.

[16] Lin Zhu, Jining He, Dianran Yan, Synthesis and microstructure observation of titanium carbonitride nanostructured coatings using reactive plasma spraying in atmosphere, Applied Surface Science 257 (20) (2011) 8722–8727.

[17] Lin Zhu, Jining He, Dianran Yan, Atmospheric reactive plasma sprayed Fe–Al_2O_3–$FeAl_2O_4$ composite coating and its property evaluation, Applied Surface Science 257 (23) (2001) 10282–10288.

[18] A. Chakraborty, A.K. Dutta, K.K. Ray, J. Surahmanya, An effort to fabricate and characterize in-situ formed graded structure in a ceramic–metal system, Journal of Materials Processing Technology 209 (5) (2009) 2681–2692.

[19] S.A. Meguid, Mechanics and mechanisms of toughening of advanced ceramics, Journal of Materials Processing Technology 56 (1–4) (1996) 978–989.